MNRAS **000**, 1–5 (2022) Preprint 13 September 2022 Compiled using MNRAS LATEX style file v3.0

# Constraints on local primordial non-Gaussianity from the large-scale clustering of DESI Luminous Red Galaxies

Mehdi Rezaie[1,2], Ashley J. Ross[3], Hee-Jong Seo[2], Hui Kong[3], Edmond Chaussidon[4], Anna Porredon[3], Lado Samushia[1], Rongpu Zhou[5], Alex Krolewski[6,7,8], Arnaud de Mattia[4], Florian Beutler[9], Christophe Yeche[4], Nathalie Palanque-Delabrouille[4,5], Klaus Honscheid[3,10], and DESI Builders

[1]*Department of Physics, Kansas State University, 116 Cardwell Hall, Manhattan, KS 66506, USA*
[2]*Department of Physics and Astronomy, Ohio University, Athens, OH 45701, USA*
[3]*Center for Cosmology and AstroParticle Physics, The Ohio State University, 191 West Woodruff Avenue, Columbus, OH 43210, USA*
[4]*IRFU, CEA, Universite Paris-Saclay, F-91191 Gif-sur-Yvette, France*
[5]*Lawrence Berkeley National Laboratory, 1 Cyclotron Road, Berkeley, CA 94720, USA*
[6]*Department of Physics and Astronomy, University of Waterloo, 200 University Ave W, Waterloo, ON N2L 3G1, Canada*
[7]*Perimeter Institute for Theoretical Physics, 31 Caroline St. North, Waterloo, ON N2L 2Y5, Canada*
[8]*Waterloo Centre for Astrophysics, University of Waterloo, 200 University Ave W, Waterloo, ON N2L 3G1, Canada*
[9]*Institute for Astronomy, University of Edinburgh, Royal Observatory, Blackford Hill, Edinburgh EH9 3HJ, UK*
[10]*Department of Physics, The Ohio State University, 191 West Woodruff Avenue, Columbus, OH 43210, USA*

Accepted XXX. Received YYY; in original form ZZZ

**ABSTRACT**

This paper uses the large-scale clustering of luminous red galaxies selected from the Dark Energy Spectroscopic Instrument Legacy Imaging Surveys Data Release 9 to constrain the local primordial non-Gaussianity (PNG) parameter $f_{\rm NL}$. Using the angular power spectrum, we thoroughly investigate the impact of various photometric systematic effects, such as those caused by Galactic extinction and varying survey depth. Simulations are utilized to construct covariance matrices, evaluate the robustness of our pipeline, and perform statistical tests to assess whether spurious fluctuations are properly mitigated and calibrated. Using modes from $\ell = 2$ to 300, we find $X1 < f_{\rm NL} < X2$ with our conservative and $X1 < f_{\rm NL} < X2$ with extreme treatment of imaging systematics, both at 68% confidence. While our results are consistent with zero PNG, but we show that the understanding of imaging systematics is of paramount importance to obtain unbiased constraints on $f_{\rm NL}$.

**Key words:** cosmology: inflation - large-scale structure of the Universe

## 1 INTRODUCTION

Current observations of the cosmic microwave background, large-scale structure, and supernovae are explained by a cosmological model that consists of dark energy, dark matter, and ordinary luminous matter, which has gone through a phase of rapid expansion known as *inflation* (see, e.g., Weinberg et al. 2013). At the end of inflation, the universe was reheated and primordial fluctuations are created to seed the subsequent growth of structure. Statistical properties of primordial fluctuations still remain as one of the unsolved puzzles in modern observational cosmology. Analyses of cosmological data have revealed that initial conditions of the universe are consistent with Gaussian fluctuations; however, there are some classes of models that predict some levels of non-Gaussianities in the primordial gravitational field.

Primordial non-Gaussianity of the local type is parameterized by Komatsu & Spergel (2001),

$$\Phi = \phi + f_{\rm NL}(\phi^2 - <\phi^2>), \quad (1)$$

where $\phi$ represents the primordial gravitational field and $f_{\rm NL}$ is the coefficient of the nonlinear correction to the primordial field. The most stringest constraints on $f_{\rm NL}$ comes from the three-point statistics of the CMB temperature anisotropies, $f_{\rm NL} = 0.9 \pm 5.0$ (Akrami et al. 2019). However, it has been shown that PNG has a scale-dependent signature on the two-point clustering of biased tracers of dark matter gravitational field. The clustering of biased tracers is boosted on large scales by a scale-dependent shift proportional to $k^{-2}$ (see, Dalal et al. 2008).

Previous studies of $f_{\rm NL}$ with galaxy and quasar clustering

have been hindered dramatically by spurious fluctuations in target density, which are due to the variation of imaging properties across the sky (Ho et al. 2015). For instance, Pullen & Hirata (2013) found that the level of systematic contamination in the quasar sample of SDSS DRX does not allow a robust $f_{\rm NL}$ measurement. These imaging systematic issues are expected to be severe for wide-area galaxy surveys that observe the night sky closer to the Galactic plane and select faint targets. Assuming imaging systematics are under control, the next generation of galaxy surveys such as DESI and the Rubin Observatory are forecast to yield unprecedented constraints on $f_{\rm NL}$. Combined with CMB data, the limits can be enhanced to a precision level required to differentiate between single and multi-field inflationary models.

In this paper, we use photometric galaxies and quasars from the DESI Legacy Imaging Surveys Data Release 9 to constrain the primordial non-Gaussianity parameter $f_{\rm NL}$, while marginalizing over bias and shotnoise parameters. We make use of spectroscopic data from DESI Survey Validation to determine the redshift distribution of galaxies. We cross correlate target density fields with the templates of imaging systematics to quantify systematic error and assess the effectiveness of systematics treatments and the significance of residual systematic error. The methodologies and statistical tools presented in this work will pave the path for future imaging surveys.

## 2 DATA

Luminous red galaxies are massive galaxies that lack active star formation and considered as one of the highly biased tracers of large scale structure. They are widely targeted in previous galaxy surveys and their clustering and redshift properties are well known. We use the photometric DESI Luminous Red Galaxies (LRG), selected from the imaging surveys (Dey et al. 2018) using color cuts described in the $g$, $r$, $z$, and $W1$ bands (see, Zhou et al. 2021), and summarized in Tab. 1. The LRG sample are masked for bright stars and foreground bright galaxies and clusters of galaxies[1], and then binned into HEALPix (Gorski et al. 2005) at NSIDE = 256 to construct the LRG density field, with an average density of 800 deg$^{-2}$ with a coverage around 14000 square degrees of the sky, as shown in Fig. 1. The density map is accounted for pixel incompleteness using a catalog of random points with the similar cuts and masks as the LRG sample.

We study the correlation between target density field and potential sources of systematic error, mapped into HEALPix similar to the data. The maps considered in this study are stellar density from Myers et al. (2022) from Gaia, Galactic extinction E[B-V] from Schlegel et al. (1998), and other systematics properties including survey depth (galaxy depth in grz and PSF depth in W1) and seeing in grz from DESI imaging. Fig. 2 shows the Spearman correlation between galaxy density and imaging properties.

Fig. **??** shows the redshift distribution of LRGs and the halo bias as a function of redshift.

[1] See https://www.legacysurvey.org/dr9/bitmasks/

## 3 METHODOLOGY

### 3.1 Measuring Power Spectrum

Galaxy density contrast in pixel $i$ is defined as,

$$\hat{\delta}_i = \frac{\rho_i}{\hat{\bar{\rho}}} - 1, \tag{2}$$

where $\rho$ is the density of galaxies accounted for pixel area $f_{{\rm pix},i}$ and $\hat{\bar{\rho}}$ is the mean galaxy density estimated by,

$$\hat{\bar{\rho}} = \frac{\sum_i \rho_i f_{{\rm pix},i}}{\sum_i f_{{\rm pix},i}}. \tag{3}$$

By definition, Eqs. 2 and 3 ensure that the integral of the observed quantity over the footprint vanishes:

$$\sum_i \hat{\delta}_i \; f_{{\rm pix},i} = 0, \tag{4}$$

To estimate power spectrum, we expand the galaxy overdensity field in terms of Legendre polynomials,

$$\hat{\delta}_i = \sum_{\ell=0}^{\ell_{\rm max}} \sum_{m=-\ell}^{\ell} a_{\ell m} Y_{\ell m}(\theta_i, \phi_i), \tag{5}$$

where $\theta, \phi$ represent the polar and azimuthal angular coordinates of pixel $i$, respectively. The cutoff at $\ell = \ell_{\rm max}$ assumes that modes with $\ell > \ell_{\rm max}$ do not contribute significantly to signal power. The coefficients $a_{\ell m}$ are then obtained by integrating the density contrast field over the total number of non-empty pixels $N_{\rm pix}$ and using the orthogonality of Legendre polynomials:

$$\hat{a}_{\ell m} = \frac{4\pi}{N_{\rm pix}} \sum_{i=1}^{N_{\rm pix}} \hat{\delta}_i \; f_{{\rm pix,i}} \; Y^*_{\ell m}(\theta_i, \phi_i), \tag{6}$$

where $^*$ represents the complex conjugate. Then, the angular power spectrum estimator is defined as the variance of $\hat{a}_{\ell m}$ coefficients:

$$\hat{C}_\ell = \frac{1}{2\ell + 1} \sum_{m=-\ell}^{\ell} \hat{a}_{\ell m} \hat{a}^*_{\ell m}. \tag{7}$$

In order to extract $\hat{a}_{\ell m}$ and compute the angular power spectrum, $C_\ell$, we make use of the ANAFAST function from HEALPix (Gorski et al. 2005) with the third order iteration of the quadrature to increase the accuracy[2]. Due to the survey geometry implicit in the summation over the non-empty pixels and explicit in $f_{\rm pix,i}$, our estimator does not return an unbiased estimate of power spectrum, and thus the same effect must be accounted in the modeling of power spectrum.

### 3.2 Modeling Power Spectrum

The projected angular power spectrum of galaxies in the presence of redshift space distortions and local primordial non-Gaussianity is related to the 3D linear power spectrum $P(k)$ and shotnoise $N_{\rm shot}$ by (see, e.g., Slosar et al. 2008),

$$C_\ell = \frac{2}{\pi} \int_0^\infty \frac{dk}{k} k^3 P(k) |\Delta_\ell(k)|^2 + N_{\rm shot}, \tag{8}$$

[2] We refer the reader to https://healpix.sourceforge.io/pdf/subroutines.pdf, p. 104-105.

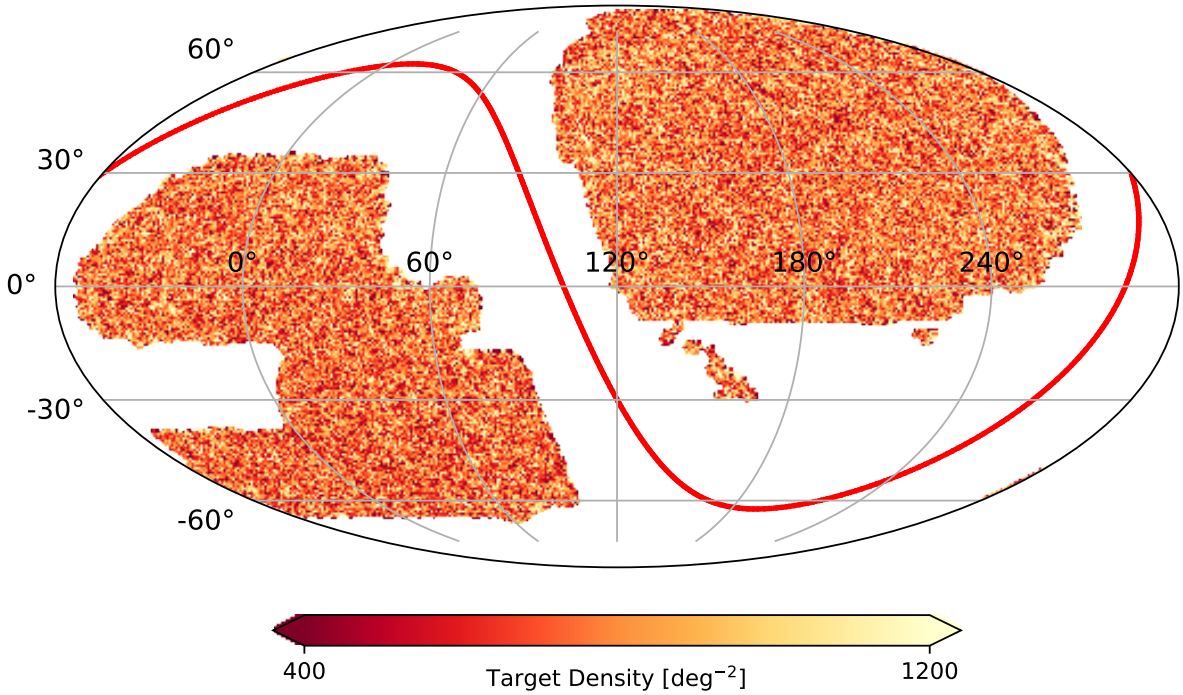


**Figure 1.** Observed density field of DESI Luminous Red Galaxies DR9 in deg$^{-2}$.

**Table 1.** Selection criteria for the LRG targets.

| Criterion | Description |
|---|---|
| **DECaLS** | |
| $z_{\rm fiber} < 21.7$ | faint limit |
| $z - W1 > 0.8 \times (r - z) - 0.6$ | Stellar rejection |
| $[(g - r > 1.3)$ AND $((g - r) > -1.55 * (r - W1) + 3.13)]$ OR $(r - W1 > 1.8)$ | Remove low-z galaxies |
| $[(r - W1 > (W1 - 17.26) * 1.8)$ AND $(r - W1 > W1 - 16.36)]$ OR $(r - W1 > 3.29)$ | Luminosity cut |
| **BASS+MzLS** | |
| $z_{\rm fiber} < 21.71$ | faint limit |
| $z - W1 > 0.8 \times (r - z) - 0.6$ | Stellar rejection |
| $[(g - r > 1.34)$ AND $((g - r) > -1.55 * (r - W1) + 3.23)]$ OR $(r - W1 > 1.8)$ | Remove low-z galaxies |
| $[(r - W1 > (W1 - 17.24) * 1.83)$ AND $(r - W1 > W1 - 16.33)]$ OR $(r - W1 > 3.39)$ | Luminosity cut |

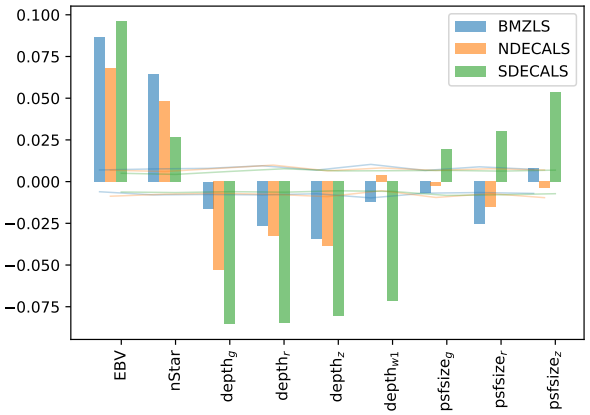


**Figure 2.** Spearman correlation coefficient between galaxy density and imaging properties.

where $\Delta_\ell(k) = \Delta^{\rm g}_\ell(k) + \Delta^{\rm RSD}_\ell(k) + \Delta^{\rm f_{NL}}_\ell(k)$ and,

$$\Delta^{\rm g}_\ell(k) = \int \frac{dr}{r} r b(r) D(r) \frac{dN}{dr} j_\ell(kr), \tag{9}$$

$$\Delta^{\rm RSD}_\ell(k) = -\int \frac{dr}{r} r f(r) D(r) \frac{dN}{dr} j''_\ell(kr), \tag{10}$$

$$\Delta^{\rm f_{NL}}_\ell(k) = f_{\rm NL} \frac{\alpha}{k^2 T(k)} \int \frac{dr}{r} r [b(r) - p] \frac{dN}{dr} j_\ell(kr), \tag{11}$$

where $\alpha = 3\delta_c \Omega_M (H_0/c)^2$, $b(r)$ is the linear bias, $dN/dr$ is the normalized redshift distribution of galaxies[3], $D(r)$ is the normalized growth factor such that $D(0) = 1$, $f(r)$ is the growth rate, and $r$ is the comoving distance. The parameter $p$ is the response of the tracer to halo's gravitational field, e.g., 1 for luminous red galaxies and 1.6 for recent mergers. In order to overcome rapid oscillations in

[3] $dN/dr = (dN/dz) * (dz/dr) \propto (dN/dz) * H(z)$

spherical Bessel functions, we employ the FFTLog[4] algorithm and its extension as implemented in **?** to compute the inner integrations over $d \ln r$.

### 3.2.1 *Survey Geometry*

For a galaxy survey that observes the sky partially, the measured power spectrum is convolved with the survey geometry. This means that the pseudo-power spectrum $\hat{C}_\ell$ obtained by the direct Spherical Harmonic Transforms of a partial sky map, differs from the full-sky angular spectrum $C_\ell$. However, their ensemble average is related by (**?**)

$$< \hat{C}_\ell >= \sum_{\ell'} M_{\ell\ell'} < C_{\ell'} >, \tag{12}$$

where $M_{\ell\ell'}$ represents the mode-mode coupling from the partial sky coverage. This is known as the Window Function effect and a proper assessment of this effect is crucial for a robust measurement of the large-scale clustering of galaxies. This window effect is a source of observational systematic error and impacts the measured galaxy clustering, especially on scales comparable to survey size.

We follow a similar approach to that of (**?**) to model the window function effect on the theoretical power spectrum $C_\ell$ rather than correcting the measured pseudo-power spectrum from data. First, we use HEALPIX to compute the pseudo-power spectrum of the window $\hat{C}_\ell^{\rm window}$, which is defined by a mask file in ring ordering format with NSIDE= 256. Then, we transform it to correlation function by,

$$\omega^{\rm window}(\theta) = \frac{1}{4\pi}\sum_\ell (2\ell+1)\hat{C}_\ell^{\rm window} P_\ell(\cos\theta). \tag{13}$$

Next, we normalize $\omega^{\rm window}$ such that it is normalized to one at $\theta = 0$. Finally, we multiply the theory correlation function by $\omega^{\rm window}$ and transform the result back to $\ell$-space,

$$\hat{\omega}^{\rm model} = \omega^{\rm model}\omega^{\rm window} \tag{14}$$

$$\hat{C}_\ell^{\rm model} = 2\pi \int d\theta \hat{\omega}^{\rm model}(\theta) P_\ell(\cos\theta). \tag{15}$$

### 3.2.2 *Integral Constraint*

The integral of the galaxy density contrast $\delta$ on the footprint is bound to zero, which is often referred to as the *Integral Constraint*. We account for this effect in the modeling by,

$$\hat{C}_\ell^{\rm model,IC} = \hat{C}_\ell^{\rm model} - \hat{C}_0^{\rm model}\left(\frac{\hat{C}_\ell^{\rm window}}{\hat{C}_0^{\rm window}}\right) \tag{16}$$

## 3.3 Characterization of systematic effects

We use the diagnostic presented in Rezaie et al 2021 based on cross power spectrum of galaxy density field and imaging maps to quantify the significance of imaging systematic effects. Taking $C_\ell^{g,x}$ as the cross power spectrum between galaxy density contrast field and imaging map, one can normalize this quantity by auto power spectrum of imaging map itself:

$$\hat{C}_{x,\ell} = \frac{(\hat{C}_\ell^{g,x})^2}{\hat{C}_\ell^{x,x}}, \tag{17}$$

and then construct a vector from cross spectra against all other imaging maps:

$$\hat{C}_{X,\ell} = [\hat{C}_{x_1,\ell}, \hat{C}_{x_2,\ell}, \hat{C}_{x_3,\ell}, ..., \hat{C}_{x_9,\ell}]. \tag{18}$$

The mean and standard deviation of $\hat{C}_{X,\ell}$ for 1000 mocks with and without $f_{\rm NL}$ are shown in Fig. 3. Finally, cross power spectrum $\chi^2$ can be defined as,

$$\chi^2 = C_{X,\ell}^T C^{-1} C_{X,\ell}, \tag{19}$$

where covariance matrix $C =< C_{X,\ell} C_{X,\ell'} >$ is constructed from mocks without systematic effects. This statistics is measured for every mock realization with the leave-one-out technique to construct a histogram, which is then compared to the $\chi^2$ value observed from the DR9.

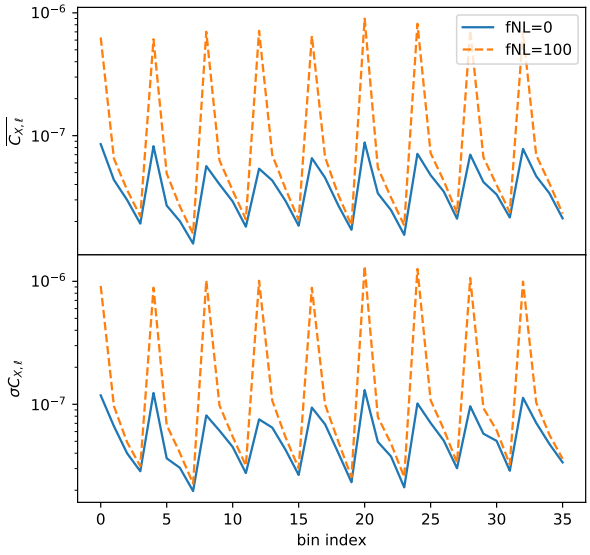


**Figure 3.** Normalized cross power spectrum of mocks. Top: mean cross spectrum. Bottom: standard deviation.

## 4 RESULTS

## 5 CONCLUSION

## ACKNOWLEDGEMENTS

## DATA AVAILABILITY

## REFERENCES

Akrami Y., et al., 2019, arXiv preprint arXiv:1905.05697
Dalal N., Dore O., Huterer D., Shirokov A., 2008, Physical Review D, 77, 123514
Dey A., et al., 2018, arXiv preprint arXiv:1804.08657
Gorski K. M., Hivon E., Banday A. J., Wandelt B. D., Hansen F. K., Reinecke M., Bartelmann M., 2005, The Astrophysical Journal, 622, 759
Ho S., et al., 2015, J. Cosmology Astropart. Phys., 2015, 040
Komatsu E., Spergel D. N., 2001, Physical Review D, 63, 063002
Pullen A. R., Hirata C. M., 2013, Publications of the Astronomical Society of the Pacific, 125, 705

[4] github.com/xfangcosmo/FFTLog-and-beyond

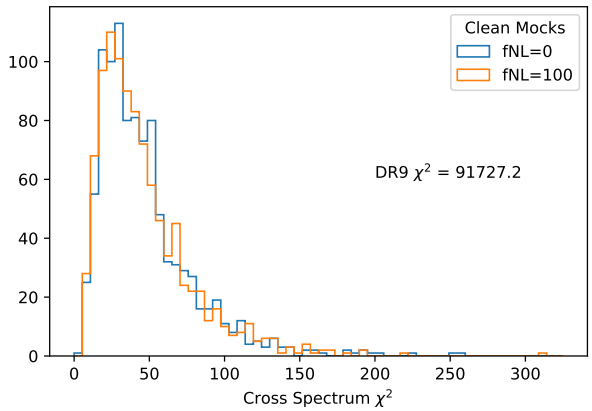


**Figure 4.** Cross power spectrum $\chi^2$ diagnostic. The DR9 value is quoted and the histograms are constructed from 1000 realizations of mocks with $f_{\rm NL} = 0$ and 100.

Schlegel D. J., Finkbeiner D. P., Davis M., 1998, The Astrophysical Journal, 500, 525

Slosar A., Hirata C., Seljak U., Ho S., Padmanabhan N., 2008, Journal of Cosmology and Astroparticle Physics, 2008, 031

Weinberg D. H., Mortonson M. J., Eisenstein D. J., Hirata C., Riess A. G., Rozo E., 2013, Physics reports, 530, 87

Zhou R., et al., 2021, Monthly Notices of the Royal Astronomical Society, 501, 3309

This paper has been typeset from a TEX/LATEX file prepared by the author.